Acta Cryst E CRYSTALLOGRAPHIC COMMUNICATIONS
ISSN 2056-9890

Synthesis and crystal structure of (2*S*,4a*R*,8a*R*)-6-oxo-2,4a,6,8a-tetrahydropyrano[3,2-*b*]pyran-2-carboxamide

John Greene,[a] Noa Kopplin,[a] Jack Roireau,[a] Mark Bezpalko,[a] Scott Kassel,[a] Michael W. Giuliano[b] and Robert Giuliano[a]*

[a]Department of Chemistry, Villanova University, 800 E Lancaster Avenue, Villanova, PA, USA, and [b]Department of Chemistry and Biochemistry, College of Charleston, 66 George Street, Charleston, SC, USA. *Correspondence e-mail: robert.giuliano@villanova.edu

Received 10 December 2019
Accepted 29 January 2020

Edited by M. Zeller, Purdue University, USA

Keywords: diplopyrone; pyranopyran; crystal structure.

CCDC reference: 1980773

Supporting information: this article has supporting information at journals.iucr.org/e

The pyranopyran amide (2*S*,4a*R*,8a*R*)-6-oxo-2,4a,6,8a-tetrahydropyrano[3,2-*b*]-pyran-2-carboxamide, $C_9H_9NO_4$, **3**, was prepared by a chemoselective hydration of the corresponding nitrile, **2**, using a heterogeneous catalytic method based on copper(II) supported on molecular sieves, in the presence of acetaldoxime. Compound **3** belongs to a new class of pyranopyrans that possess antibacterial and phytotoxic activity. Crystallographic analysis of **3** shows a bent structure for the *cis*-fused bicyclic pyranopyran, similar to nitrile **2**. Evidence of an intramolecular hydrogen bond involving the amide group and ring oxygen was not observed; however, two separate intermolecular hydrogen-bonding interactions were observed between the amide hydrogen atoms and adjacent carbonyl oxygen atoms along the *b*- and *a*-axis directions. The latter interaction may also be supported by an intermolecular C—H···O hydrogen bond. The lattice is filled out by close-packed layers of this hydrogen-bonded network along the *c*-axis direction, related from one to the next by a 2_1 screw axis.

1. Chemical context

The phytotoxin diplopyrone **1** was isolated from the fungus *Diplodia mutila* and reported in 2003 (Evidente *et al.*, 2003). This fungus is considered a causative agent of cork oak decline and diplopyrone is implicated as the main phytotoxin responsible for this disease, the economic and environmental impacts of which are well known (Giorgio *et al.*, 2005). The proposed structure of diplopyrone contains a *cis*-fused pyranopyran core and four chirality centers, originally assigned as 9*S*,6*R*,8a*S*,4a*S*, but revised recently to 9*R*,6*S*,8a*S*,4a*S* (Fusè *et al.*, 2019). In 2019, our laboratory published the synthesis and biological evaluation of pyranopyran analogs based on the structure of diplopyrone (Lazzara *et al.*, 2019). These enantiomeric analogs showed antibacterial and phytotoxic activity, in one case exceeding the activity of a commercially used antibiotic that is used to treat bacterial diseases in pond-raised catfish, which is the largest segment of aquaculture in the United States. Pyranopyran nitrile **2** was approximately 100 times more potent in bioassay than florfenicol against *Edwardsiella ictaluri*, which causes enteric septicemia (ESC), a disease that can result in losses of tens of millions of dollars to the industry annually. Compound **2** was also phytotoxic in an assay using the aquatic plant *Lemna paucicostata* (L.) Hegelm. (duckweed). As part of our ongoing efforts to synthesize additional analogs of **1** for testing as new antibacterials and herbicides, we have recently

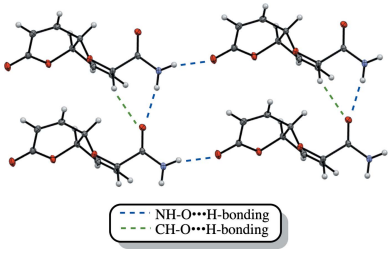

prepared amide **3**, by a heterogeneous catalytic method that uses copper(II) supported on molecular sieves, in the presence of acetaldoxime to carry out chemoselective hydration of **2** (Kiss & Hell, 2011).

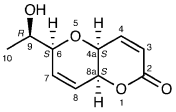

(+)–Diplopyrone (**1**)

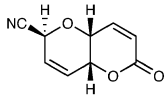

Pyranopyran Nitrile (**2**)

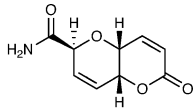

Pyranopyran Amide (**3**)

2. Structural commentary

Pyranopyrans in which the two rings are *cis*-fused are relatively rare compared to *trans*-fused pyranopyrans (Giuliano, 2014). A consequence of the *cis* ring fusion is that the molecule has more of a bent shape than it would if *trans*-fused, which is demonstrated by the O1—C8*A*—C4*A*—O5 torsion angle of 72.95 (15)° *versus* 177° for a comparable *trans*-fused pyranopyran (Yu *et al.*, 2017). Both rings adopt half-chair conformations, placing the amide group in a near 1,3-diaxial interaction with H4*A*. These features are consistent with the results in the computational study reported (Evidente *et al.*, 2003). The study suggests the hydroxyethyl side chain is involved in an intramolecular hydrogen bond between the hydroxyl group and the O5 ring oxygen. By contrast, the amide side chain in **3** does not exhibit a similar intramolecular hydrogen bond with its amino group in the solid state, as shown in Fig. 1. The overall structure of **3** is nearly identical to that of the pyranopyran nitrile **2** with obvious deviation at the side chain.

The NMR spectra of the pyranopyran amide **3** are similar to those of pyranopyran nitrile **2**. The most obvious difference in the ^{13}C spectra is the presence of the additional (amide) carbonyl carbon in **3** at δ 174.1 ppm and the absence of the nitrile carbon that occurs at δ 114.9 in **2**. The ^{1}H spectrum of **3** shows slight changes in the chemical shifts of most protons, for example there is a downfield shift of H4*A* from δ 4.45 ppm in the nitrile to δ 4.61 ppm in the amide. The vinyl hydrogen H4 is also further downfield in the amide (δ 7.10 ppm *vs* 6.91 ppm). The torsion angle of 45.8° for H4*A*—C4*A*—C8*A*—H8*A* in **3** is consistent with the observed vicinal coupling constant of 4.5 Hz for H4*A*—H8*A* in the associated ^{1}H NMR spectrum.

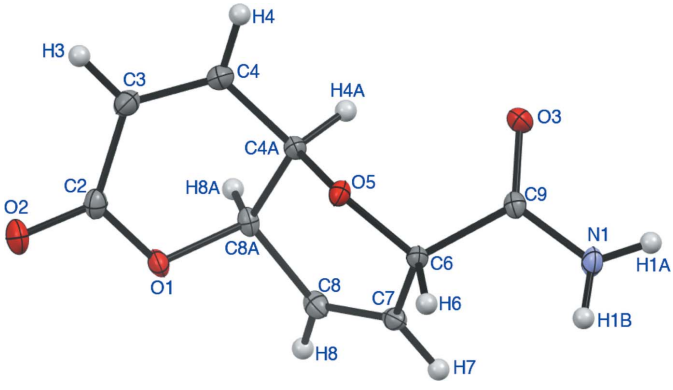

Figure 1
Molecular structure of **3** with displacement ellipsoids at the 50% probability level.

Table 1
Hydrogen-bond geometry (Å, °).

D—H···*A*	*D*—H	H···*A*	*D*···*A*	*D*—H···*A*
N1—H1*A*···O2^{i}	0.86 (3)	2.08 (3)	2.8840 (18)	156 (2)
N1—H1*B*···O3^{ii}	0.87 (2)	2.21 (2)	3.0462 (18)	163.1 (19)
C6—H6···O3^{ii}	1.00	2.52	3.2787 (19)	133

Symmetry codes: (i) $x, y+1, z$; (ii) $x+1, y, z$.

3. Supramolecular features

The amino hydrogen atoms of **3** are involved in intermolecular hydrogen bonding with adjacent carbonyl oxygen atoms: H1*A* with O2^{i} and H1*B* with O3^{ii} (Fig. 3, Table 1, Symmetry codes: (i) $x, y+1, z$; (ii) $x+1, y, z$.). A packing diagram of **3** (Fig. 2*a*) shows the N—H···O hydrogen-bonding interactions forming molecular planes defined by the crystallographic *a*- and *b*-axes; packing of these hydrogen-bonded layers appears to be a function of solvent exclusion and van der Waals contact alone, lacking any hydrogen bonding.

The hydrogen-bonded network in the *ab* plane also presents an arrangement of C—H···O and C—H···π interactions that suggests two potential additional forces at play within the lattice of **3**. Fig. 2*b* and Table 1 depict distances between H6 and O3^{ii} and C6 and O3^{ii} of adjacent copies of **3**. These distances fall within parameters for C—H···O hydrogen bonding as has been described in well-characterized membrane proteins and peptidomimetics (Senes *et al.*, 2001; Giuliano *et al.*, 2009); the α-protons implicated in these systems are structurally analogous to the C6—H6 bond of **3**. While we will not speculate on the energetic significance of this interaction, which can arise as a coincidence of crystal packing (Dunitz & Gavezzotti, 2005), we note that such interactions have been spectroscopically measured within the core of the dimeric membrane peptide glycophorin A (Arbely & Arkin, 2004). Further, solid-state NMR studies have observed that ^{1}H and ^{13}C NMR shifts change for anomeric C—H bonds in crystalline maltose samples, suggesting that such interactions as described in this study (the C6—H6 bond in **3** is pseudo-anomeric) are not consequences of an energetically dominant lattice arrangement and N—H···O hydrogen bonding, but rather have some measurable, albeit weak, energetic contribution to intermolecular association (Yates *et al.*, 2005).

Within the *ab* plane, H4*A* of one copy of **3** comes into close approach with its closest neighbor along the *a* axis. Fig. 3*c* depicts these distances, which place the centroid of the C7=C8 double bond within distance parameters similar to those calculated for aliphatic C—H···π interactions (Karthikeyan *et al.*, 2013). We investigated this further using a semi-empirical protocol to generate partial charges for the atoms of **3**. This only allows for qualitative comparison, and, as the color coding in Fig. 2*c* reveals, the C7=C8 bond (pink, negative) is electrostatically matched with H4*A* (light blue,

positive). Proper exploration of this would require more advanced QM/MM methods, however, the crystal packing of **3** is at least suggestive of a favorable geometry and electrostatic environment for C—H···π interactions.

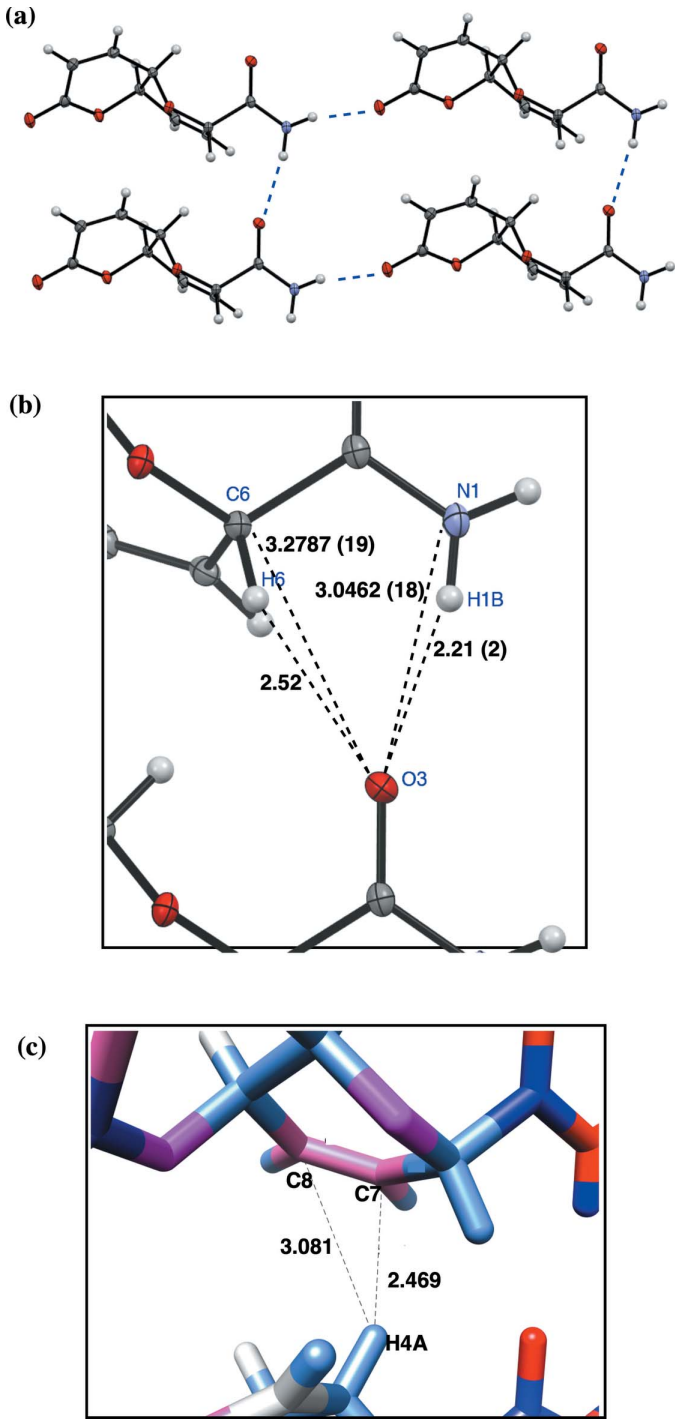

Figure 2
(*a*) Hydrogen-bonding interactions between copies of **3** along the *a* and *b* axes. (*b*) C—O and H—O distances suggestive of a potential C—H···O hydrogen bond along the *a* axis. N—H···O distances for the H1*B*···O3 hydrogen bond are included for comparison. (*c*) Measured distances and electrostatic coloring between H4*A*, C7, and C8 used to explore a potential C—H···π interaction within the *ab* plane molecular layers. Partial charges were generated within UCSF Chimera (Pettersen *et al.*, 2004) using the Amber ff14SB forcefield in Antechamber (Wang *et al.*, 2006) with the semi-empirical AM1 – BCC method and color coded with pink for negative charges and light blue for positive charges.

4. Database survey

A search of the Cambridge Structural Database (CSD Version 5.41, November 2019; Groom *et al.*, 2016) using the core fused ring lactone in the search query revealed only three similar structures (Somarathne *et al.*, 2019; Lazzara *et al.*, 2019) in which the pyranopyran ring system is *cis*-fused and the two double bonds are in the same location as they are in **3**. Among the total 40 structures that were found in the search, the pyranopyran core of several were *trans*-fused, for example, the bergenins and also truncated ladder ethers related to brevitoxin. Some compounds possessed aryl rings fused to the pyranopyran system while others had double bonds at alternate positions including the ring junction.

5. Synthesis and crystallization

(2*S*,4a*R*,8a*R*)-6-Oxo-2,4a,6,8a-tetrahydropyrano[3,2-*b*]pyran-2-carboxamide 3:

Compound **3** was prepared by the procedure of Kiss & Hell (2011) with a change of solvent from methanol to *tert*-butanol. A mixture of (4a*R*,6*S*,8a*R*)-6-cyano-6,8a-dihydropyrano-[3,2-*b*]pyran-2-(4a*H*)-one **2** (0.040 g, 0.226 mmol), Cu^{II}-4 Å catalyst (0.022 g), acetaldoxime (0.040 g, 0.678 mmol) and *tert*-butanol (2 mL) was stirred at 343 K for 4 h. The mixture was filtered through a pad of Celite and concentrated to a yellow–brown solid that was purified by cartridge chromatography on a Waters vacuum manifold system using 5% methanol/chloroform as eluant (flash chromatography was also successful using 10% methanol/chloroform). Concentration of fractions left a white solid; yield, 0.0227 g (51.5%). Single crystals were obtained from a solution of **3** in 10% methanol/chloroform at 253 K. R_f = 0.2 (10% methanol/ chloroform); mp 433-437 K; $[\alpha]_D^{20}$ −268 (*c*, 0.8, methanol); IR (ATR) ν 3425, 3325, 3219, 1710, 1670, 1618 cm^{-1}; ^1H NMR (300 MHz, $CDCl_3$) δ 7.10 (*dd*, 1H, $J_{3,4}$ = 10.1, $J_{4,4a}$ = 5.4 Hz, H-4), 6.40 (*ddd*, 1H, $J_{7,8}$ = 10.2, $J_{6,7}$ = 3.6, $J_{7,8a}$ = 1.2 Hz, H-7), 6.16 (*d*, 1H, $J_{3,4}$ = 10.5, H-3), 6.10 (*m*, 1H, H-8), 4.86 (*bs*, 2H, NH_2), 4.80 (*m*, 2H, H-6, H-8a), 4.61 (*ddd*, 1H, $J_{4a,4}$ = $J_{4a,8a}$ = 4.5, $J_{4a,8}$ = 1.2 Hz, H-4a); $^{13}C\{^1H\}$ NMR ($CDCl_3$) δ 174.1, 164.8, 143.7, 131.8, 124.5, 123.3, 74.0, 70.2, 64.4. HRMS (ESI–TOF) *m*/*z* calculated for $C_9H_{10}NO_4$ 196.0610, found 196.0607.

6. Refinement

Crystal data, data collection, and structure refinement details are summarized in Table 2. The absolute configuration was known from the synthetic route and assigned accordingly. The amino hydrogen atoms were found in the electron difference map and refined isotropically, while all other hydrogen atoms were treated as idealized contributions with C—H = 0.95–1.00 Å and U_{iso}(H) = 1.2U_{eq}(C).

Table 2
Experimental details.

Crystal data	
Chemical formula	$C_9H_9NO_4$
M_r	195.17
Crystal system, space group	Orthorhombic, $P2_12_12_1$
Temperature (K)	100
a, b, c (Å)	4.9279 (1), 10.6350 (3), 15.8788 (4)
V (Å^3)	832.18 (4)
Z	4
Radiation type	Mo $K\alpha$
μ (mm^{-1})	0.12
Crystal size (mm)	0.4 × 0.3 × 0.18
Data collection	
Diffractometer	Bruker SMART APEXII area detector
Absorption correction	Multi-scan (*SADABS*; Krause *et al.*, 2015)
T_{min}, T_{max}	0.654, 0.746
No. of measured, independent and observed [$I > 2\sigma(I)$] reflections	14252, 2461, 2366
R_{int}	0.031
(sin $\theta/\lambda)_{max}$ (Å^{-1})	0.708
Refinement	
$R[F^2 > 2\sigma(F^2)]$, $wR(F^2)$, S	0.032, 0.080, 1.04
No. of reflections	2461
No. of parameters	135
H-atom treatment	H atoms treated by a mixture of independent and constrained refinement
$\Delta\rho_{max}$, $\Delta\rho_{min}$ (e Å^{-3})	0.35, −0.20
Absolute structure	Flack x determined using 928 quotients $[(I^+)-(I^-)]/[(I^+)+(I^-)]$ (Parsons et al., 2013)
Absolute structure parameter	−0.1 (3)

Computer programs: *APEX3* (Bruker, 2016), *SAINT* (Bruker, 2015), *SIR92* (Altomare *et al.*, 1994), *SHELXL2014* (Sheldrick, 2015) and *OLEX2* (Dolomanov *et al.*, 2009).

Funding information

The authors thank Villanova University for financial support of this work.

References

Altomare, A., Cascarano, G., Giacovazzo, G., Guagliardi, A., Burla, M. C., Polidori, G. & Camalli, M. J. (1994). *Appl. Cryst.* **27**, 435.

Arbely, E. & Arkin, I. T. (2004). *J. Am. Chem. Soc.* **126**, 5362–5363.

Bruker (2015). *SAINT*. Bruker AXS Inc., Madison, Wisconsin, USA.

Bruker (2016). *APEX3*. Bruker AXS Inc., Madison, Wisconsin, USA.

Dolomanov, O. V., Bourhis, L. J., Gildea, R. J., Howard, J. A. K. & Puschmann, H. (2009). *J. Appl. Cryst.* **42**, 339–341.

Dunitz, J. D. & Gavezzotti, A. (2005). *Angew. Chem. Int. Ed.* **44**, 1766–1787.

Evidente, A., Maddau, L., Spanu, E., Franceschini, A., Lazzaroni, S. & Motta, A. (2003). *J. Nat. Prod.* **66**, 313–315.

Fusè, M., Mazzeo, G., Longhi, G., Abbate, S., Masi, M., Evidente, A., Puzzarini, C. & Barone, V. (2019). *J. Phys. Chem. B*, **123**, 9230–9237.

Giorgio, E., Maddau, L., Spanu, E., Evidente, A. & Rosini, C. (2005). *J. Org. Chem.* **70**, 7–13.

Giuliano, M. W., Horne, W. S. & Gellman, S. H. (2009). *J. Am. Chem. Soc.* **131**, 9860–9861.

Giuliano, R. M. (2014). *Curr. Org. Chem.* **18**, 1686–1700.

Groom, C. R., Bruno, I. J., Lightfoot, M. P. & Ward, S. C. (2016). *Acta Cryst.* B**72**, 171–179.

Karthikeyan, S., Ramanathan, V. & Mishra, B. K. (2013). *J. Phys. Chem. A*, **117**, 6687–6694.

Kiss, A. & Hell, Z. (2011). *Tetrahedron Lett.* **52**, 6021–6023.

Krause, L., Herbst-Irmer, R., Sheldrick, G. M. & Stalke, D. (2015). *J. Appl. Cryst.* **48**, 3–10.

Lazzara, N. C., Rosano, R. J., Vagadia, P. P., Giovine, M. T., Bezpalko, M. W., Piro, N. A., Kassel, Wm. S., Boyko, W. J., Zubris, D. L., Schrader, K. K., Wedge, D. E., Duke, S. O. & Giuliano, R. M. (2019). *J. Org. Chem.* **84**, 666–678.

Parsons, S., Flack, H. D. & Wagner, T. (2013). *Acta Cryst.* B**69**, 249–259.

Pettersen, E. F., Goddard, T. D., Huang, C. C., Couch, G. S., Greenblatt, D. M., Meng, E. C. & Ferrin, T. E. (2004). *J. Comput. Chem.* **25**, 1605–1612.

Senes, A., Ubarretxena-Belandia, I. & Engelman, D. M. (2001). *Proc. Natl Acad. Sci. USA*, **98**, 9056–9061.

Sheldrick, G. M. (2015). *Acta Cryst.* C**71**, 3–8.

Somarathne, K. K., McCone, J. A. J., Brackovic, A., Rivera, J. L. P., Fulton, J., Russell, E., Field, J. J., Orme, C. L., Stirrat, H. L., Riesterer, J., Teesdale–Spittle, P. H., Miller, J. H. & Harvey, J. E. (2019). *Chem. Asian J.* **14**, 1230–1237.

Wang, J., Wang, W., Kollman, P. A. & Case, D. A. (2006). *J. Mol. Graphics Modell.* **25**, 247–260.

Yates, J. R., Pham, T. N., Pickard, C. J., Mauri, F., Amado, A. M., Gil, A. M. & Brown, S. P. (2005). *J. Am. Chem. Soc.* **127**, 10216–10220.

Yu, K., Wu, W., Li, S., Dou, L., Liu, L., Li, P. & Liu, E. (2017). *Nat. Prod. Res.* **31**, 2581–2586.

supporting information

Acta Cryst. (2020). E**76**, 761-764 [https://doi.org/10.1107/S2056989020001292]

Synthesis and crystal structure of (2*S*,4a*R*,8a*R*)-6-oxo-2,4a,6,8a-tetrahydropyrano[3,2-*b*]pyran-2-carboxamide

John Greene, Noa Kopplin, Jack Roireau, Mark Bezpalko, Scott Kassel, Michael W. Giuliano and Robert Giuliano

Computing details

Data collection: *APEX3* (Bruker, 2016); cell refinement: *SAINT* (Bruker, 2015); data reduction: *SAINT* (Bruker, 2015); program(s) used to solve structure: *SIR92* (Altomare *et al.*, 1994); program(s) used to refine structure: *SHELXL2014* (Sheldrick, 2015); molecular graphics: *OLEX2* (Dolomanov *et al.*, 2009); software used to prepare material for publication: *OLEX2* (Dolomanov *et al.*, 2009).

(2*S*,4a*R*,8a*R*)-6-Oxo-2,4a,6,8a-tetrahydropyrano[3,2-*b*]pyran-2-carboxamide

Crystal data

$C_9H_9NO_4$
M_r = 195.17
Orthorhombic, $P2_12_12_1$
a = 4.9279 (1) Å
b = 10.6350 (3) Å
c = 15.8788 (4) Å
V = 832.18 (4) Å^3
Z = 4
$F(000)$ = 408
D_x = 1.558 Mg m^{-3}
Mo $K\alpha$ radiation, λ = 0.71073 Å
Cell parameters from 8408 reflections
θ = 2.3–30.2°
μ = 0.12 mm^{-1}
T = 100 K
Prism, colourless
0.4 × 0.3 × 0.18 mm

Data collection

Bruker SMART APEXII area detector diffractometer
Radiation source: sealed tube
Graphite monochromator
Detector resolution: 8 pixels mm^{-1}
ω and φ scans
Absorption correction: multi-scan (SADABS; Krause *et al.*, 2015)
T_{min} = 0.654, T_{max} = 0.746
14252 measured reflections
2461 independent reflections
2366 reflections with $I > 2\sigma(I)$
R_{int} = 0.031
θ_{max} = 30.2°, θ_{min} = 2.3°
h = −5→6
k = −15→14
l = −22→22

Refinement

Refinement on F^2
Least-squares matrix: full
$R[F^2 > 2\sigma(F^2)]$ = 0.032
$wR(F^2)$ = 0.080
S = 1.04
2461 reflections
135 parameters
0 restraints
Primary atom site location: structure-invariant direct methods
Hydrogen site location: mixed
H atoms treated by a mixture of independent and constrained refinement
$w = 1/[\sigma^2(F_o^2) + (0.0446P)^2 + 0.205P]$ where $P = (F_o^2 + 2F_c^2)/3$
$(\Delta/\sigma)_{max} < 0.001$

$\Delta\rho_{max}$ = 0.35 e Å^{-3}
$\Delta\rho_{min}$ = −0.20 e Å^{-3}

Absolute structure: Flack *x* determined using 928 quotients [(I^+)-(I^-)]/[(I^+)+(I^-)] (Parsons et al., 2013)
Absolute structure parameter: −0.1 (3)

Special details

Geometry. All esds (except the esd in the dihedral angle between two l.s. planes) are estimated using the full covariance matrix. The cell esds are taken into account individually in the estimation of esds in distances, angles and torsion angles; correlations between esds in cell parameters are only used when they are defined by crystal symmetry. An approximate (isotropic) treatment of cell esds is used for estimating esds involving l.s. planes.

Refinement. 1. Fixed Uiso At 1.2 times of: All C(H) groups 2.a Ternary CH refined with riding coordinates: C4A(H4A), C6(H6), C8A(H8A) 2.b Aromatic/amide H refined with riding coordinates: C3(H3), C4(H4), C7(H7), C8(H8) 3. N1(H1A) and N1(H1B) located from the difference map with refined Uiso

Fractional atomic coordinates and isotropic or equivalent isotropic displacement parameters (Å²)

	x	*y*	*z*	U_{iso}*/U_{eq}
O1	0.7129 (2)	0.30730 (10)	0.31022 (7)	0.0145 (2)
C2	0.5987 (3)	0.22091 (15)	0.36070 (9)	0.0141 (3)
O2	0.7069 (3)	0.11890 (11)	0.36663 (8)	0.0198 (3)
C3	0.3563 (3)	0.25659 (15)	0.40997 (9)	0.0155 (3)
H3	0.2482	0.1928	0.4350	0.019*
C4	0.2869 (3)	0.37655 (14)	0.41980 (10)	0.0154 (3)
H4	0.1413	0.3982	0.4562	0.019*
C4A	0.4377 (3)	0.47756 (14)	0.37369 (9)	0.0121 (3)
H4A	0.3071	0.5453	0.3574	0.015*
O5	0.6340 (2)	0.52880 (10)	0.43085 (6)	0.0118 (2)
C6	0.7796 (3)	0.63226 (13)	0.39613 (9)	0.0107 (3)
H6	0.9519	0.6405	0.4289	0.013*
C7	0.8579 (3)	0.61248 (14)	0.30510 (9)	0.0126 (3)
H7	0.9754	0.6718	0.2792	0.015*
C8	0.7700 (3)	0.51613 (14)	0.25988 (9)	0.0140 (3)
H8	0.8362	0.5046	0.2042	0.017*
C8A	0.5687 (3)	0.42536 (14)	0.29495 (9)	0.0124 (3)
H8A	0.4244	0.4103	0.2518	0.015*
C9	0.6280 (3)	0.75809 (14)	0.40406 (8)	0.0112 (3)
O3	0.3793 (2)	0.76516 (11)	0.40436 (7)	0.0163 (2)
N1	0.7940 (3)	0.85729 (13)	0.40610 (9)	0.0151 (3)
H1A	0.735 (5)	0.933 (2)	0.4068 (15)	0.033 (6)*
H1B	0.967 (5)	0.845 (2)	0.4125 (13)	0.017 (5)*

Atomic displacement parameters (Å²)

	U^{11}	U^{22}	U^{33}	U^{12}	U^{13}	U^{23}
O1	0.0173 (5)	0.0092 (5)	0.0170 (5)	0.0032 (4)	0.0028 (4)	−0.0007 (4)
C2	0.0161 (7)	0.0111 (7)	0.0151 (6)	−0.0009 (5)	−0.0026 (5)	−0.0014 (5)
O2	0.0235 (6)	0.0102 (5)	0.0255 (6)	0.0034 (4)	0.0003 (5)	0.0013 (4)
C3	0.0137 (6)	0.0138 (7)	0.0189 (7)	−0.0026 (6)	0.0003 (5)	0.0016 (6)
C4	0.0121 (6)	0.0140 (7)	0.0202 (7)	−0.0014 (5)	0.0027 (5)	−0.0012 (5)
C4A	0.0104 (6)	0.0093 (6)	0.0166 (6)	0.0006 (5)	0.0004 (5)	−0.0011 (5)

O5	0.0140 (5)	0.0093 (5)	0.0121 (4)	−0.0021 (4)	0.0006 (4)	0.0006 (4)
C6	0.0103 (6)	0.0087 (6)	0.0130 (6)	−0.0001 (5)	−0.0001 (5)	0.0005 (5)
C7	0.0116 (6)	0.0119 (6)	0.0145 (6)	0.0021 (5)	0.0030 (5)	0.0029 (5)
C8	0.0170 (7)	0.0133 (7)	0.0117 (6)	0.0035 (6)	0.0023 (5)	0.0018 (5)
C8A	0.0153 (7)	0.0088 (6)	0.0130 (6)	0.0021 (5)	−0.0017 (5)	−0.0005 (5)
C9	0.0144 (6)	0.0096 (6)	0.0097 (5)	0.0009 (5)	0.0001 (5)	−0.0001 (5)
O3	0.0121 (5)	0.0128 (5)	0.0240 (5)	0.0019 (4)	0.0016 (4)	−0.0016 (4)
N1	0.0155 (6)	0.0082 (6)	0.0215 (6)	0.0000 (5)	−0.0023 (5)	0.0015 (5)

Geometric parameters (Å, º)

O1—C2	1.3428 (18)	C6—H6	1.0000
O1—C8A	1.4629 (18)	C6—C7	1.511 (2)
C2—O2	1.2126 (19)	C6—C9	1.538 (2)
C2—C3	1.478 (2)	C7—H7	0.9500
C3—H3	0.9500	C7—C8	1.324 (2)
C3—C4	1.330 (2)	C8—H8	0.9500
C4—H4	0.9500	C8—C8A	1.492 (2)
C4—C4A	1.497 (2)	C8A—H8A	1.0000
C4A—H4A	1.0000	C9—O3	1.2280 (19)
C4A—O5	1.4343 (18)	C9—N1	1.335 (2)
C4A—C8A	1.513 (2)	N1—H1A	0.86 (3)
O5—C6	1.4243 (17)	N1—H1B	0.87 (2)
C2—O1—C8A	118.85 (12)	C7—C6—C9	108.88 (11)
O1—C2—C3	118.63 (14)	C9—C6—H6	107.1
O2—C2—O1	118.31 (14)	C6—C7—H7	118.6
O2—C2—C3	122.97 (14)	C8—C7—C6	122.88 (13)
C2—C3—H3	119.5	C8—C7—H7	118.6
C4—C3—C2	121.08 (14)	C7—C8—H8	119.5
C4—C3—H3	119.5	C7—C8—C8A	121.06 (13)
C3—C4—H4	119.9	C8A—C8—H8	119.5
C3—C4—C4A	120.23 (14)	O1—C8A—C4A	112.66 (12)
C4A—C4—H4	119.9	O1—C8A—C8	107.10 (12)
C4—C4A—H4A	108.9	O1—C8A—H8A	108.7
C4—C4A—C8A	110.65 (12)	C4A—C8A—H8A	108.7
O5—C4A—C4	107.33 (12)	C8—C8A—C4A	110.78 (12)
O5—C4A—H4A	108.9	C8—C8A—H8A	108.7
O5—C4A—C8A	112.00 (12)	O3—C9—C6	122.57 (14)
C8A—C4A—H4A	108.9	O3—C9—N1	124.26 (15)
C6—O5—C4A	112.85 (11)	N1—C9—C6	113.09 (13)
O5—C6—H6	107.1	C9—N1—H1A	122.5 (17)
O5—C6—C7	113.04 (12)	C9—N1—H1B	118.8 (14)
O5—C6—C9	113.33 (12)	H1A—N1—H1B	118 (2)
C7—C6—H6	107.1		
O1—C2—C3—C4	−15.0 (2)	O5—C4A—C8A—C8	−47.00 (16)
C2—O1—C8A—C4A	41.32 (17)	O5—C6—C7—C8	8.0 (2)

C2—O1—C8A—C8	163.37 (12)	O5—C6—C9—O3	−30.03 (19)
C2—C3—C4—C4A	6.2 (2)	O5—C6—C9—N1	153.21 (13)
O2—C2—C3—C4	161.46 (16)	C6—C7—C8—C8A	4.7 (2)
C3—C4—C4A—O5	−98.05 (16)	C7—C6—C9—O3	96.70 (16)
C3—C4—C4A—C8A	24.4 (2)	C7—C6—C9—N1	−80.06 (15)
C4—C4A—O5—C6	−176.04 (11)	C7—C8—C8A—O1	−108.78 (16)
C4—C4A—C8A—O1	−46.75 (16)	C7—C8—C8A—C4A	14.4 (2)
C4—C4A—C8A—C8	−166.70 (12)	C8A—O1—C2—O2	173.12 (13)
C4A—O5—C6—C7	−41.21 (16)	C8A—O1—C2—C3	−10.21 (19)
C4A—O5—C6—C9	83.29 (14)	C8A—C4A—O5—C6	62.33 (15)
O5—C4A—C8A—O1	72.95 (15)	C9—C6—C7—C8	−118.85 (16)

Hydrogen-bond geometry (Å, º)

D—H···*A*	*D*—H	H···*A*	*D*···*A*	*D*—H···*A*
N1—H1*A*···O2^{i}	0.86 (3)	2.08 (3)	2.8840 (18)	156 (2)
N1—H1*B*···O3^{ii}	0.87 (2)	2.21 (2)	3.0462 (18)	163.1 (19)
C6—H6···O3^{ii}	1.00	2.52	3.2787 (19)	133

Symmetry codes: (i) *x*, *y*+1, *z*; (ii) *x*+1, *y*, *z*.